Freie Universität Berlin

Title:

Coupled Methyl Group Rotation in FMN Radicals Revealed by Selective Deuterium Labeling

Author(s):

Richard Brosi, Boris Illarionov, Lorenz Heidinger, Ryu-Ryun Kim, Markus Fischer, Stefan Weber, Adelbert Bacher, Robert Bittl, and Erik Schleicher

Document type: Preprint

Coupled Methyl Group Rotation in FMN Radicals Revealed by Selective Deuterium Labeling

Richard Brosi,[†] Boris Illarionov,[‡] Lorenz Heidinger,[§] Ryu-Ryun Kim,[‡] Markus Fischer,[‡] Stefan Weber,[§] Adelbert Bacher,[‡,‖] Robert Bittl[†] and Erik Schleicher*[§]

[†] Freie Universität Berlin, Fachbereich Physik, Institut für Experimentalphysik, Arnimallee 14, 14195 Berlin, Germany.

[‡] Universität Hamburg, Institut für Lebensmittelchemie, Grindelallee 117, 20146 Hamburg, Germany.

[§] Albert-Ludwigs-Universität Freiburg, Institut für Physikalische Chemie, Albertstr. 21, 79104 Freiburg, Germany.

[‖] Fakultät für Chemie, Technische Universität München, Lichtenbergstr. 4, 80247 Garching, Germany

Abstract Flavin semiquinones are common intermediate redox states in flavoproteins, and thus, knowledge of their electronic structure is essential for fully understanding their chemistry and chemical versatility. In this contribution, we use a combination of high-field ENDOR

spectroscopy and selective deuterium labeling of flavin mononucleotide (FMN) with subsequent incorporation as cofactor into a variant *Avena sativa* LOV domain to extract missing traits of the electronic structure of a protein-bound FMN radical. From these experiments, precise values of small proton hyperfine and deuterium nuclear quadrupole couplings could be extracted. Specifically, isotropic hyperfine couplings of −3.34 MHz, −0.11 MHz and +0.91 MHz were obtained for the protons H(6), H(9) and H(7α), respectively. These values are discussed in the light of specific protein-cofactor interactions. Furthermore, the temperature behavior of the H(7α) methyl-group rotation elicited by its energy landscape was analyzed in greater detail. Pronounced interplay between the two methyl groups at C(7) and C(8) of FMN could be revealed. Most strikingly, this rotational behavior could be modulated by selective deuterium editing.

Introduction

Flavoproteins belong to the large family harboring derivatives of riboflavin, FMN and/or FAD, as cofactors. They are involved in a wide variety of enzyme-catalyzed redox transformations, and can act as photoreceptor chromophores.[1-3] The redox-active part of the cofactor is the 7,8-dimethyl isoalloxazine moiety that is able to adopt three different oxidation states: fully reduced, semiquinone (radical), and fully oxidized, with various degrees of protonation. Flavoproteins not only engage in hydride transfer, but also in one-electron transfer reactions,[1-3] the latter resulting in flavin semiquinone species as reaction intermediates. Neutral and anionic flavin radicals have been investigated for decades both in isotropic solution[4] and incorporated in proteins.[5] Particular attention was given to the electronic structures and charge distributions within the isoalloxazine

moiety as knowledge on the electron-spin density distribution is considered essential for understanding the chemical reactivity of the isoalloxazine ring and its versatility in different protein environments. Since the flavin semiquinone state is paramagnetic with spin quantum number $S = 1/2$, electron paramagnetic resonance (EPR) and related methods play pivotal roles in its characterization.[5-7] Although tremendous experimental progress has been made in recent years, knowledge of the electronic structure of flavin radicals is still incomplete.[8]

The anisotropic electron Zeeman interaction, parameterized by the **g** tensor, and electron–nuclear hyperfine (hf) couplings (hfcs) $\mathbf{A}_i$ of the unpaired electron spin to nearby magnetic nuclei *i* are sensitive reporters of the electronic structure of a radical in general, and a flavin radical in particular. Hfcs reflect the unpaired electron-spin density at the positions of magnetic nuclei. They are directly correlated with the probability density of the electronic wave function. The parameters **g** and $\mathbf{A}_i$ can be accurately measured using EPR and electron-nuclear double resonance (ENDOR).[9-10] Up to now, however, hyperfine analyses of flavins were in most cases restricted to the protons that carry high electron-spin density and correspondingly have large hfcs, such as H(8α) or H(5).[6, 11-15] Resonances arising from smaller hfcs of protons with lower electron-spin densities (such as H(7α) and H(9)) strongly overlap in conventional ENDOR experiments and conglomerate to the so-called matrix-ENDOR line. Although rough estimates of hfcs from these protons are available in the literature for some flavoproteins,[16] an unambiguous signal assignment of all proton hfcs from the 7,8-dimethyl isoalloxazine moiety could not be achieved up to now.

To overcome this unfortunate situation, we applied a novel strategy to measure and assign proton hfcs of a neutral flavin radical in its native protein environment by a combination of high-microwave-frequency ENDOR and selective deuterium editing of the cofactor. In principle, a

disentanglement of ^{2}H-ENDOR signals from the resonances of other magnetic nuclei can be achieved under high-magnetic-field conditions where the Larmor precessional frequencies of the involved nuclei become increasingly different. This allows for a precise measurement of ^{2}H hfcs due to reduced spectral overlap. Furthermore, pulsed ENDOR performed at high magnetic fields provides improved spectral resolution and, due to the pronounced **g**-tensor anisotropy of the radical, enables the selection of molecules with a specific orientation with respect to the direction of the external magnetic field, even in a non-oriented sample. Due to the small **g**-tensor anisotropy of flavin radicals,[17] however, distinct orientation selection is typically observed at microwave frequencies of around 90 GHz or larger.

As model flavoprotein, the LOV2 domain from *Avena sativa* phototropin was selected for the present study. LOV domains are modular blue-light sensing domains found in many organisms including plants and certain prokaryotes.[18-21] Structurally, LOV domains are members of the PAS superfamily[22] comprising about 100 amino acids, which noncovalently bind an FMN molecule as light-sensitive cofactor. Phototropins are able to sense an external physical stimulus – light – via their LOV domains and convert it into a biological signal that propagates to downstream reactions via their reporter domain. Blue-light perception by LOV domains is responsible for numerous phenomena including phototropism, chloroplast movement, stomatal opening, regulation of virulence and general stress response.[23-25]

The primary photochemical reaction after blue-light illumination of LOV domains involves the formation of a covalent adduct (the so-called flavin–cysteinyl C(4a) adduct) between the FMN cofactor and a neighboring strictly conserved cysteine residue,[26-29] presumably via a transiently formed cysteine-FMN radical pair.[28] When the cognate cysteine residue is exchanged, e.g., for alanine or serine, adduct formation is inhibited, and instead a metastable neutral FMN radical is

formed by light-induced electron transfer that decays within tens of seconds to minutes at ambient temperature.[29-32]

Recently, we examined different neutral FMN radicals (FMNH$^\bullet$) in LOV domains with regard to their temperature behavior by using X-band ENDOR spectroscopy at cryogenic temperatures.[33] In one of the cysteine-exchanged LOV domains, C450A LOV2 from *A. sativa* (LOV*), we detected a quite unusual behavior of one of the two methyl groups in the isoalloxazine moiety, namely the 8α-methyl group.[33] Downward from approximately 100 K, the rotation of the methyl group stalled within the ENDOR time scale of several microseconds. Moreover, mutational studies of three amino acids surrounding the 8α-methyl group led to the identification of one amino acid that critically influences both the rotation of the methyl group and the biologically relevant dark-state recovery of the LOV* domain. Hence, we could demonstrate that protein cofactor interactions significantly modulate the photoreaction of the photoreceptor. This work was recently repeated with an engineered LOV photoreceptor YF1 and with flavodoxin, both investigated proteins showed similar behavior.[34-35]

With the present contribution, we expand our knowledge on this phenomenon by investigating the 7α methyl group attached to C(7). We were particularly interested in answering the question, whether the 7α methyl group exhibits a similar response to a temperature variation as does the adjacent 8α-methyl group. Hence, we reinvestigated the LOV* protein with ENDOR spectroscopy at low temperatures. The electron spin density situated on the three 7α methyl-group protons is supposed to be small as measurements of the isotropic hyperfine coupling using photo-CIDNP imply.[36] Therefore, their ENDOR resonances are expected to overlap with those of other nuclei with small proton hfcs in the matrix ENDOR line. The anisotropy of the 7α proton hfc has not yet been assigned experimentally. To do so, the more sophisticated aforementioned

approach, a combination of selective deuterium labeling, cofactor exchange, and high-field ENDOR spectroscopy is essential to extract these resonances. As an important fringe benefit of this concept, all other small, yet unassigned, proton hfcs become accessible.

Experimental Section

Isotope labeling.

[6,8α-^{2}H$_4$]Riboflavin, [9,7α-^{2}H$_4$]riboflavin and [6,7α,8α,9-^{2}H$_8$]riboflavin (see Scheme 1 for details) were prepared according to published procedures.[37] NMR and mass spectroscopy confirmed the deuterium labeling of the three isotopologs (Figures S8–S10 and Tables S5 and S6).

Preparation of labeled FMN.

A reaction mixture (total volume, 20 ml) containing 100 mM Tris-hydrochloride, pH 8.0, 10 mM magnesium chloride, 0.02 % sodium azide, 5 mM dithiothreitol, 0.5 mM ATP, 6 mM phosphoenol pyruvate, 0.5 mM riboflavin, 5 units of pyruvate kinase from rabbit muscle (Sigma) and 2 mg of recombinant riboflavin kinase from *Schizosaccharomyces pombe* was incubated at 310 K. The progress of the reaction was monitored by thin layer chromatography (microcrystalline cellulose plates, Macherey-Nagel; eluent, 350 mM phosphate, pH 7.0). When the riboflavin had mostly disappeared (typically after about 12 h), the reaction mixture was evaporated to dryness under reduced pressure and stored at 77 K.

Protein production and reconstitution with FMN isotopologs.

The recombinant *Escherichia coli* strain M15 harboring the plasmids pREP4 and pNCO-HISLOVWT [29] was grown in LB medium at 303 K. Frozen cell mass (6 g) was suspended in 50 ml of 50 mM Tris hydrochloride, pH 7.0, containing 300 mM NaCl, 20 mM imidazole and 0.02 % sodium azide (buffer A). Lysozyme (5 mg), DNase I (5 mg) and phenylmethanesulfonyl fluoride (0.5 mM) were added. The mixture was incubated at room temperature for 30 min while stirring and was then passed through a French Press. Cell debris was removed by centrifugation, and the supernatant was placed on the top of a Chelating Sepharose column (Ni^{2+} form, 2×5 cm) that had been equilibrated with the same buffer. The column was washed with 5 column volumes of buffer A and with 3 volumes of buffer A containing 6 M guanidine hydrochloride or until the effluent had become colorless, and then buffer A (15 ml) containing 4 mg of isotopically labeled FMN was circulated through the column overnight under protection from light. The column was washed with buffer A and was then developed with 100 ml of buffer A with a linear gradient of imidazole (20 mM–1 M). Fractions were combined, concentrated to a volume of 2 ml and transferred to buffer B (50 mM Tris hydrochloride pH 7.5, 200 mM KCl, 2.5 mM $CaCl_2$, 0.02% NaN_3) by ultrafiltration. Thrombin (150 units) was added, and the mixture was incubated at 25 °C for 12 h and was then passed through a Chelating Sepharose column (Ni^{2+} form, 2×5 cm) equilibrated with buffer A. The effluent was concentrated, transferred to buffer C (50 mM K/Na-phosphate pH 7.0, 0.02% NaN_3) by ultrafiltration, and stored at 77 K.

EPR sample preparation.

Samples containing 10 mM HEPES, pH 7.0, 10 mM NaCl, 30 % glycerol (v/v), 5 mM EDTA and 0.5–0.7 mM protein were transferred into W-band EPR quartz tubes (0.3 mm inner diameter) in the dark. Subsequent blue light illumination using a narrow-banded LED (3 W, 455 nm, FWHM 20 nm) generated the semi-reduced state of the FMN cofactor (FMNH$^\bullet$). Reaction progress was monitored using a Varian Cary 100 spectrophotometer. Samples were frozen rapidly and stored in liquid nitrogen.

W-band Mims ENDOR spectroscopy.

W-band pulsed ENDOR spectra were recorded using a commercial pulse EPR spectrometer Bruker E680 (Bruker BioSpin GmbH, Rheinstetten, Germany). W-band pulsed ENDOR spectra were obtained using a DICE-II ENDOR accessory and a radio-frequency (RF) amplifier (Amplifier Research 150A400). The EPR/ENDOR resonator (Bruker Teraflex EN600-1021H) was immersed in a helium gas flow cryostat (Oxford CF-960) regulated by a temperature controller (Oxford ITC-503). Pulsed W-band EPR spectra were recorded using a ($\pi/2$) pulse of 24 ns and a separation time of 500 ns. For Mims-type ENDOR spectroscopy, a microwave pulse sequence ($\pi/2$)–τ–($\pi/2$)–T (with RF-pulse)–($\pi/2$) with 24-ns $\pi/2$-pulses, respectively, and an RF pulse starting 1 µs after the second microwave pulse were used. The separation times τ and T were set to 700 ns and 54 µs, respectively, the RF pulse length was 52 µs. The experiment was repeated with a duty cycle of 100 Hz at 80 K and only 5 Hz at 20 K to account for prolonged relaxation times at lower temperatures. Performing the low-temperature experiments at 20 K instead of 10 K, as in an earlier publication,[33] provided significantly better temperature stability over time without altering the spectral shape in the W-band ENDOR spectra. In order to examine orientation selection, two magnetic field positions were selected at the maximum of the field-

swept echo (g_{max}) and one at g_z, except when otherwise noted. Magnetic-field swept electron-spin echo detected EPR spectra were recorded using a ($\pi/2$)–500 ns–π microwave-pulse sequence with 64-ns and 128-ns $\pi/2$- and π-pulses, respectively.

X-band Davies ENDOR spectroscopy.

The experimental setup for pulsed Davies-type ENDOR at X-band frequencies is described elsewhere.[33]

Data analysis.

Typically, ENDOR data were recorded at two different magnetic field positions. These correspond to the case, where the molecules are aligned with their *x*- and *y*-, or with their *z*-axis parallel to the external magnetic field. Spectral simulations to extract hfcs were carried out using the Matlab (The MathWorks, Natick, MA) package EasySpin (using the "saffron" simulation routine for Mims ENDOR);[38] the manual optimization was performed with a self-written Matlab script. For extraction of the respective deuterium hfcs, the following procedures were carried out: Published hfcs from density functional theory (DFT) calculations (at the B3LYP/EPR-II level of theory) of a neutral FADH$^{\bullet}$ were used as starting parameters.[39] These parameters were optimized manually, and special emphasis was taken to optimize not only the intensity, but also the shape of the signal. Consequently, the error analysis was carried out individually for all signals (Table 1). ENDOR linewidths were chosen independently for each deuteron: 0.03 MHz for D(6), 0.023 MHz for D(9), 0.06 MHz for D(7α) and 0.1 MHz for D(8α). W-band pulsed-EPR linewidth was 0.45 mT.

DFT calculations.

The rotational barriers of both methyl groups of the 7,8-dimethylisoalloxazine moiety of FMN were calculated on the level of DFT using the ORCA program toolbox.[40] The flavin structure was taken from the pdb file 1CZU[41] and the ribityl side chain was truncated to CH_3. This structure was fully geometry optimized *in vacuo* using the BP86 functional and the Def2-TZVP basis set (see Supporting Information for details). Thereafter, the dihedral angle (defined by the atoms C(8), C(7), C(7α) and H(7α)) was fixed and the 8α-CH_3 group rotated to obtain the rotational barrier of the 8α-CH_3 group. Only C(8), C(8α), and all hydrogens were allowed to relax. This procedure was repeated for the 7α group, keeping the dihedral angle of the 8α group fixed and rotating the 7α group. In this case, only C(7), C(7α), and all hydrogens were allowed to relax. In the next step, the influence of each CH_3 group was tested by first replacing either the 7α-CH_3 group or the 8α-CH_3 group with hydrogen. Again, a full geometry optimization was applied. The rotational barrier of the 8α group in the absence of the 7α-group was calculated by keeping all atoms fixed, except C(8), C(8α) and all hydrogens. The same procedure was applied vice versa (see Figures S4–S7). For all barrier calculations, the BP86 functional and the Def2-SVP Basis-set was used. The dihedral angels were incremented in 3°, 5° or 10°-steps. For details see SI.

Results

Assignment of deuteron hyperfine couplings.

Figure 1 depicts the W-band EPR spectrum of the neutral FMN radical in [6,7α,8α,9-$^2H_8$]FMN-reconstituted *As*LOV2-C450A ([xylene-$^2H_8$]LOV*), together with its spectral simulation. Similar to other flavoprotein radicals, the principal components of the **g**-tensor are

not fully resolved at this microwave frequency.[42-44] Despite the intrinsically broad spectrum caused by the anisotropy of **g**, the lineshape with the emerging structure is mainly due to the large hfcs of the atoms N(5), N(10) and H(5). It is noteworthy, that the hyperfine pattern arising from the hfcs of these nuclei appears in general better resolved in [xylene-^{2}H$_8$]LOV* than in non-labeled samples (see e.g., [42, 45]) because of the absence of hfcs from the nuclei H(6), H(7α), H(8α) and H(9).

EPR parameters were obtained by spectral simulation. We used published EPR parameters for a neutral flavin radical: a **g**-tensor with principal values of 2.0043, 2.0036 and 2.0022, and hfcs (0, 0, 50.1 MHz), (0, 0, 31.7 MHz), and (−8.5, −37, −24.9 MHz) for the nuclei N(5), N(10) and H(5), respectively.[14, 43] The agreement between experiment and simulation is remarkably good.[33] This is strong indication that our protein refolding procedure resulted in a bound FMN cofactor. Although the overall shape of the EPR spectrum with its maxima and minima is described quite well by the simulations, slight deviations remain. These can be rationalized by non-ideal microwave pulses that are not treated well by the simulation routine, by nuclear modulations over the magnetic-field range, or by a small contamination of unlabeled FMNH$^\bullet$ molecules in the reconstituted LOV protein sample. In the latter case, this fraction of molecules cannot be detected in deuteron-selective EPR/ENDOR experiments and thus, was ignored in further analyses.

- Please insert Figure 1 around here -

W-band Mims-ENDOR spectra of differently stable-isotope labeled LOV* samples were recorded and spectral simulations performed to extract the deuteron hfcs compiled in Table 1. These will be discussed in more detail below. In principle, hfcs extracted from orientation-selective ENDOR spectra recorded at magnetic field positions, where $\boldsymbol{B}_0$ is parallel to either one of the principal axes of the **g**-tensor (*x, y or z*, with principal values g_x, g_y, or g_z, respectively) of the paramagnetic flavin cofactor, are denoted A_x, A_y, and A_z. These components are the projections of the hfc tensor **A** of a given nucleus along *x*, *y*, and *z*, respectively, and constitute the principal values of **A** in the special case of collinear principal axes systems of **g** and **A**. In the present case, assuming collinear *z*-principal axes of **g** and **A**, we included an angle of $\delta = 17°$ between their *x*-axes as obtained from previous high-field EPR experiments.[17, 42-43, 46] From sets of these spectra, hfc components of a specific nucleus can be directly read out from the splitting between associated hf resonances. As a **g** tensor of near axial symmetry is assumed ($g_x \approx g_y$),[17] all investigated samples were recorded only at two magnetic-field positions, one at the maximum of the EPR spectrum (further denoted as g_{max}), where g_x and g_y almost resonate equally, and one at the g_z position.

In the Mims-ENDOR spectra of [xylene-$^2H_8$]LOV*, recorded at magnetic-field positions corresponding to g_{max} and a temperature of 20 K, several pairs of distinct hfcs are observed (Figure 2, upper panel). The pair of lines with the largest hfc of about 2.0 MHz with broad shoulders are from two (of three) magnetically nonequivalent deuterons attached to C(8α) if one assumes an arrested methyl group rotation.[29, 33] Notably, the hfc of the third deuteron $^2H(8α)_3$ is expected to be very small and the corresponding resonances are expected to be obscured by those from other deuterons with small hfcs that conglomerate to the matrix ENDOR line; hence, an assignment is ambiguous with this sample. Several additional features at approximately 0.8 MHz

and 0.55 MHz, and a broad one at approximately 0.4 MHz, can be detected. The spectrum of the [xylene-^{2}H$_8$]LOV* sample, recorded at the g_z position, shows a similar picture: One broad pair of signals at around 2.0 MHz arising from the two ^{2}H(8α) deuterons and two additional sharp signals centered at 1.1 MHz and 0.8 MHz, respectively (Figure 2, lower panel). In contrast to the spectrum recorded at g_{max} position, only weak resonances are observed close to the deuteron free Larmor precessional frequency of 22.0 MHz).

- Please insert Figure 2 around here -

Spectral simulations of the two unambiguously assigned ^{2}H(8α) deuterons afforded principal hfc values of A_x = 1.77 MHz, A_y = 1.90 MHz, A_z = 2.21 MHz for deuteron ^{2}H(8α)$_1$ and A_x = 1.26 MHz, A_y = 1.55 MHz and A_z = 1.77 MHz for deuteron ^{2}H(8α)$_2$, which is in excellent agreement with our previous X-band Davis-ENDOR analysis of proton hfcs.[33] The spectra recorded at two different canonical orientations of the **g**-tensor are clearly dissimilar due to the above-mentioned orientation-selection effects. The additional signals are believed to arise from the deuterons ^{2}H(6), ^{2}H(7α) and ^{2}H(9). Quantum-chemical calculations of neutral flavin radicals predict A_{iso} values for ^{2}H(6) in the range of –0.75 MHz, for ^{2}H(7α) at around –0.1 MHz, and for ^{2}H(9) at 0.2 MHz.[8, 39, 47] Although we suppose that the pair of resonances at 0.8 MHz arises from ^{2}H(6), an unambiguous assignment of the rather complex and overlapping hf pattern is not possible. Therefore, application of more selective isotope editing is an obvious requirement.

For this purpose, two additional samples, [6,8α-^{2}H$_4$]FMN and [7α,9-^{2}H$_4$]FMN were synthesized, incorporated into *As*LOV2 (further denoted as [6,8α-^{2}H$_4$]LOV* and [7α,9-^{2}H$_4$]LOV*, respectively) and investigated with Mims-ENDOR under otherwise identical experimental conditions. The resulting spectra are depicted in Figures 3 and 4. In general, the labeling efficiency of the two samples is very good, as confirmed by adding up the Mims-ENDOR spectra of the [6,8α-^{2}H$_4$]LOV* and [7α,9-^{2}H$_4$]LOV* samples and subsequent comparison with the respective [xylene-^{2}H$_8$]LOV* (see Figure S1 for details).

The spectra from [xylene-^{2}H$_8$]LOV* and [6,8α-^{2}H$_4$]LOV* exhibit several significant differences: First, the two signals centered at 0.55 MHz and 0.4 MHz are missing in the spectrum of [6,8α-^{2}H$_4$]LOV* recorded at g_{max}, and second, the broad signal located close to the ^{2}H free Larmor frequency is missing in the spectrum recorded at g_z. We therefore conclude that (i) hfcs arising from ^{2}H(7α) and ^{2}H(9) are smaller than 0.6 MHz, and (ii) all signals located within a range of 1 MHz can be attributed to ^{2}H(6) under the assumption that the signal intensity of the yet unassigned ^{2}H(8α)$_3$ is very weak due to the Mims hole close to 0 MHz.[33]

- Please insert Figure 3 around here -

Reasonable fitting results for ^{2}H(6) could only be obtained with hf values of $A_x = -0.90$ MHz, $A_y = 0.30$ MHz and $A_z = -0.94$ MHz in the simulations of the spectrum recorded at g_{max}. We note that from the spectral simulations the signs of the principal components cannot be obtained; therefore, they were taken from DFT calculations. In the spectrum recorded at g_z, however, the

pair of signals centered at 1 MHz is not reproduced convincingly with these hf values. The only rational approach is to include another interaction: nuclear quadrupole coupling (nqc).

In general, nuclei with $I \geq 1$ (such as deuterons) have an electric quadrupole moment so that their energies are split by an electric field gradient, induced, e.g., by the electronic bonds in the local environment. The theory of the quadrupolar interaction in EPR spectroscopy is outlined in detail elsewhere.[48] In EPR studies, the quadrupole tensor elements P_i are measured. For $I = 1$ nuclei, such as deuterons, they are related to the nuclear quadrupole coupling constants: $2P_i = e^2 q_i Q/h$ ($e^2 q_i$ is the largest electric-field gradient and Q is the scalar nuclear quadrupole moment). It has been shown for hydrogen-bonded aromatic molecules that the largest component of the quadrupole tensor, $P_z = V_z$, (V_i values are the principal values of the electric field gradient tensor) approximately points along the direction of the H-bond, and P_y and P_x are parallel and perpendicular to the plane of the hydrogen-bond donor molecule, respectively.[49] In general, trends in nqc and the asymmetry parameter η, which resembles the deviation of the quadrupolar tensor from axial symmetry, can be rationalized in terms of nuclear charge, bond distance (X–^{2}H), and local symmetry: a shorter bond results in a larger nqc because the nuclear contribution is larger; η is zero if the symmetry of the electric field gradient at the deuteron is high.

In the present case, a splitting of 120 kHz due to nqc is observed in the spectrum recorded at g_z (see Figure 3, lower panel). In the spectrum recorded at g_{max}, however, the sharp resonance of ^{2}H(6) located at 0.90 MHz clearly rules out a nqc that is larger than the spectral linewidth of ~40 kHz. For a more detailed analysis, we recorded a series of ENDOR spectra at magnetic field positions of g_x, g_y and g_z, and a temperature of 120 K (see Figure S2). As outlined earlier, the three deuterons attached to C(8α) are magnetically equivalent at this temperature and can be

described with one hf tensor of axial symmetry (see Table 1 for details). Therefore, the hf tensor of ^{2}H(6) is fully visible under these experimental conditions. Here, adequate spectral simulations can only be obtained if a nqc of approximately 120 kHz is assumed for the g_y direction, which leads to a Q-value of 0.1 MHz and an η value of 0.8 for ^{2}H(6) (Table 2).

The last yet unassigned hf tensor that should be visible in the two spectra depicted in Figure 3 is the third deuteron, ^{2}H(8α)$_3$. For the assignment of the small hf resonances from this nucleus, we made the following assumptions: (i) A_{iso} of the freely rotating 8α methyl group carrying ^{1}H nuclei is known from independent measurements: (7.9±0.1) MHz,[33] (ii), the full **A** tensor of the rigid deuterons ^{2}H(8α)$_1$ and ^{2}H(8α)$_2$ is very well described with the parameters depicted in Table 1, (iii), the anisotropy of the three deuteron **A**-tensors is similar, and (iv), the angle between the C(8α)–H-bond and the isoalloxazine's π-system is, as predicted from DFT calculations, around 10°.[33] With these assumptions, the hfc components $A_x = -0.32$ MHz, $A_y = 0.25$ MHz and $A_z = 0.18$ MHz, yielding an A_{iso} value of 0.08 MHz, are obtained. Although the error margins of these values had to be increased (see Table 1), both the positive sign of A_{iso} and the negative sign of A_x are mandatory for a reasonable fit of the experimental line shape.

Only hf resonances within a range of 0.6 MHz are visible in the two spectra of [7α,9-^{2}H$_4$]LOV*, recorded at magnetic fields corresponding to g_{max} and g_z (see Figure 4). In the spectrum recorded at g_{max}, two maxima, a rather sharp one at 0.59 MHz and one that is slightly broader at about 0.25 MHz can be detected. In the spectrum recorded at g_z, on the other hand, only one signal close to the free deuteron Larmor frequency is observed, which exhibits a total width of 0.5 MHz and has a shoulder at 0.25 MHz. Although DFT calculations[39] suggest and photo-CIDNP studies confirm that the hf tensor of ^{2}H(9) is generally larger than that from the

three ^{2}H(7α) nuclei,[36] an unequivocal assignment of the individual hf principal values is not possible from these two spectra alone.

- Please insert Figure 4 around here -

Consequently, a second series of ENDOR spectra was recorded with the sample at five different magnetic-field positions at 120 K (Figure 5). Here, notable changes in the individual hf resonances are observed: First, the pronounced hf resonance at 0.59 MHz remains unaltered at magnetic-field positions corresponding to g_x (and, to a lesser extent at magnetic-field positions corresponding to g_y), but disappears at magnetic-field positions close to g_z. On the other hand, the maximum and the shape of the second hf resonance at 0.2 MHz changes significantly on variation of the magnetic field. The only reasonable explanation for these findings is that signals from the smaller hf tensor belong to the three deuterons attached to C(7α) when motional dynamics are present. This observation is consistent with the recently detected temperature behavior of the 8α methyl group (see Ref. [33] and also below): While at 20 K, the three deuterons do not rotate within the time scale of the ENDOR experiment, rotation is unrestricted at 120 K. As a result, the three deuterons become magnetically equivalent and merge into one tensor of axial symmetry. The isotropic part of the hf tensor of a freely-rotating methyl group is described as the average of the three individual proton hf tensors $A_{\mathrm{iso,meth}} = (A_{\mathrm{iso,1}} + A_{\mathrm{iso,2}} + A_{\mathrm{iso,3}})/3$. The same relation applies to a deuterated methyl group. Therefore, the resonances from the three 7α deuterons vary depending on the chosen experimental conditions (Figures 4 and 5).

With these two well-defined boundary conditions, spectral simulations of the two deuteron positions 7α and 9 were conducted. As a result, the hf tensor of ^{2}H(9) had principal values of $A_x = -0.59$ MHz, $A_y = 0.33$ MHz and $A_z = 0.21$ MHz, which correspond to a very small A_{iso} value of -0.01 MHz (see Table 1). A small quadrupole coupling constant of $Q = -0.02$ MHz and an anisotropy factor of $\eta = -0.8$ was included in the simulations (Table 2, please note that these values only apply if the linewidth of the ^{2}H(9) hf-coupling components is kept as small as possible). Because of the Pake-like pattern of the ^{2}H(9) resonance, the sign of A_x has to be different from that of A_y and A_z.[50] The hf tensor of the rotating deuterons ^{2}H(7α) can be described as a quasi-axial tensor with the principal values of $A_x = -0.09$ MHz, $A_y = 0.03$ MHz and $A_z = 0.21$ MHz, yielding an A_{iso} value of 0.14 MHz (see Table 1). Because of the low intensity of hf resonances close to the free Larmor frequency of deuterons, however, increased error margins have to be assumed.

In order to determine whether the temperature behaviors of the two methyl groups are similar, Mims-ENDOR spectra were additionally recorded at 20 K and compared to those recorded at 120 K (Figure S3). Differences can be clearly observed, and are particularly apparent in the spectrum g_{max}, where the pronounced coupling at 0.2 MHz decreases substantially. This behavior is similar to the temperature behavior of the 8α methyl group protons; hence, no additional hfcs can be detected in the spectrum recorded at 20 K, which would arise from the now magnetically non-equivalent 7α methyl protons. Additionally, it is difficult to perform meaningful spectral simulations of the 7α methyl group resonances, as the area around 0 MHz does not show any ENDOR resonances due to a Mims hole, and therefore any spectral simulation would be fraught with substantial uncertainties. However, using the A-values of the H(7α) hfcs measured at 120 K

and the already introduced relation between the hfc strength of rotating and arrested 7α methyl-group deuterons, all three arrested ^{2}H(7α) hfcs can be estimated (Table 1).

Influence of the 7α methyl group on the rotation of the 8α methyl group.

To analyze interactions between 7α- and 8α-methyl group protons (and/or the respective deuterons), we further investigated the [7α,9-^{2}H$_4$]LOV* sample. X-band Davis-ENDOR spectra were recorded at two temperatures, 50 K and 150 K, and were compared with spectra recorded using an unlabeled sample under otherwise identical conditions (see Figure 6 and Ref. [33]). The concept of this experiment is to correlate the temperature dependence of the 8α-methyl group rotation with one altered "parameter", an either protonated or deuterated 7α-methyl group in its direct vicinity. As depicted in Figure 6, the Davis-ENDOR spectra of both samples are similar, but show differences upon closer inspection, which are visualized by the difference of the two spectra depicted in blue. In the difference spectrum obtained at 150 K, one small but rather sharp deviation from zero, located at a hfc of 8.5 MHz, is observed (Figure 6, upper panel). As resonances from the protons at C(7α) do not show up in this area, this deviation can be assigned to changes of the proton at C(8α). On the other hand, several small but distinct changes in the hf structure can be detected in the difference recorded at 50 K (Figure 6, lower panel). In detail, clear changes show up in the area where the three now magnetically inequivalent 8α protons are in resonance. A previous study using the same LOV protein could revealed that such shifts in hyperfine couplings are due to different angles of the methyl group relative to the isoalloxazine ring.[33] Additional deviations from zero can be detected close to the proton Larmor frequency, which could be assigned to the three 7α deuterons (Table 1).

Discussion

Assignments of hyperfine couplings of $^2H(6)$, $^2H(7\alpha)_3$, $^2H(8\alpha)_3$ and $^2H(9)$.

Until now, no unequivocal assignment of proton hfcs attached to the carbons C(6), C(7α) and C(9) in a protein-bound flavin radical has been achieved. This is due to the small isotropic hyperfine coupling constants of these protons in combination with their large hyperfine anisotropy that results in strong spectral overlap of their resonances in ENDOR spectra even at high magnetic fields. With our strategy of selective deuterium labeling, we shift specific resonances into a different ENDOR frequency range, thus allowing an unambiguous assignment. Because of the need for enhanced spectral resolution for the separation of proton and deuteron hfcs, and to exploit orientation-selection effects, the high magnetic fields applied at W-band microwave frequencies are mandatory. In this contribution, we focus on hfcs from protons (deuterons) that are at positions of low electron spin density in the 7,8-dimethyl isoalloxazine ring, and consequently, they exhibit small hfcs. Hence, the Mims-ENDOR pulse sequence was our prime choice.[51] In preliminary experiments, the length of the delay time τ was optimized to shift the ineluctable "Mims holes" to radio frequencies where no hfcs of interest are encountered. Choosing a value of 700 ns turned out to be optimal (see Figures 2 and 3).

Next, full hf tensors of $^2H(6)$, $^2H(7\alpha)_3$, $^2H(8\alpha)_3$ and $^2H(9)$ were extracted by spectral simulations. The data, together with their respective scaled proton hfcs, are summarized in Table 1. Guided by DFT calculations, the three principal components of the $^2H(6)$ hf tensor including their signs and the strength of the nqc (see also below) could be assigned with high accuracy as the spectral overlap with resonances from other deuterons is negligible in the [6,8α-$^2H_4$]LOV* sample. Previous hyperfine studies dealt with the couplings of H(6); X-band proton

Davies-ENDOR experiments were used in most of them (see, e.g., [11, 29, 33, 52-54]). Typically, only one component of the H(6) hf tensor was reported and attributed to the A_{iso} value. The H(6) hf interaction was proposed to be nearly isotropic in some studies, which is neither consistent with the predicted behavior for a proton directly attached to the π-system [55] nor with published DFT predictions.[39, 47] Martinez and coworkers presented an alternative approach by application of HYSCORE spectroscopy at X-band.[8] The authors were able to extract the anisotropic part of the H(6) hf tensor of the flavin in *Anabaena* flavodoxin and suggested full rhombicity. Results from our experiments, however, show a H(6) hf tensor of almost perfect axial symmetry with the smallest A_{iso} value ever reported from a neutral flavin radical (see Ref. [8] for a summary of experimental data from other protein-bound flavins and Table 1): whereas published experimental A_{iso} values range from $\approx |4.3 \text{ MHz}|$ in *Vibrio cholera* NADH:quinone oxidoreductase[44] to $\approx |6 \text{ MHz}|$ in *Azotobacter vinelandii* NADPH dehydrogenase,[56] the A_{iso} value of the neutral FMNH• radical in LOV* is (-3.34 ± 0.07) MHz. Whether our A_{iso} value can be attributed to an unusually low spin-density distribution at the H(6) position, or to an incomplete characterization of the hf tensor in other flavin radicals cannot be decided conclusively without further experimental data. Recent QM/MM calculations performed on the neutral flavin radical in glucose oxidase predicted A_{iso} values between -3.13 and -3.55 MHz, thus suggesting that the here reported small A_{iso} value is not unique.[57]

The principal hf components of the third deuteron attached to the 8α-methyl group, ^{2}H(8α)$_3$, could be allocated from the examination of the [6,8α-^{2}H$_4$]LOV* sample (see Table 1). Because signals arising from this hf tensor are close to the deuteron Larmor frequency and therefore exhibit a rather low signal-to-noise ratio, larger error margins were assumed and the signs of the individual components remain arguable (see Table 1). However, we are confident that the A_{iso}

value is positive, and the shape of the $^2H(8\alpha)_3$ resonance requires a sign change of at least one principal component of the hf tensor.

Mims-ENDOR spectra of the [7α,9-$^2H_4$]LOV* sample revealed the full hf tensor of the position 9 deuteron including some peculiarities: The isotropic hyperfine coupling constant A_{iso} of the proton is –0.11 MHz and much smaller than predictions from quantum chemical calculations (1.7 MHz). The shape of the tensor is less axial than that of $^2H(6)$. Although the signs of the principal components could not be directly obtained from our experiments, and could in principle be opposite, we are certain from spectral simulations that there has to be a change in sign between the A_x and the A_y/A_z components.

Last, Mims-ENDOR spectra of the [7α,9-$^2H_4$]LOV* sample, recorded at two different temperatures (20 K and 150 K), revealed the full hf tensor of the methyl group deuterons attached to C(7α). By analysis of data obtained at different temperatures, both the axial tensor of the freely-rotating methyl group as well as the individual hf tensors from the rotationally arrested individual protons could be extracted (see Table 1). Previous studies using cw-ENDOR spectroscopy with unlabeled flavoproteins afforded only an estimate of A_{iso} values of the H(7α) methyl group at elevated temperatures.[16] In summary, only by exploiting selective $^1H{\to}^2H$ replacement in combination with high-field EPR spectroscopy, the complete hf tensors of protons/deuterons that harbor small electron-spin density in flavins become accessible.

Quadrupole coupling

Although the nqc is an intrinsic part of the spin Hamiltonian in magnetic-resonance studies of nuclei with nuclear spin quantum numbers ≥1, this interaction is often treated subordinately. Up to now, most experimental values have been obtained from NMR and quadrupole spectroscopy

of diamagnetic molecules. ^{2}H nqcs in spatially rigid C–^{2}H bonds show a dependence on the hybridization of the carbon nucleus: for sp^3 sites, nqcs around 170–175 kHz, for sp^2 sites 180–185 kHz and for sp sites >200 kHz have been reported.[58-60] Molecular motion, or more precisely movement of the C–^{2}H bond with respect to the external magnetic field, will cause a reduction of these values. The fast rotation of methyl groups (around the pseudo-threefold spinning axis) in organic solids at elevated temperatures results in nqcs in the 45–55-kHz range with an anisotropy factor close to zero.[61-62] Therefore, we expect no sizeable nqc in ENDOR resonances from the two methyl groups.

Few experimental values of nqcs have been reported from deuterated protein samples in their paramagnetic states. One example is the EPR/ENDOR spectroscopic analysis performed on the quinone acceptor site of the reaction center from the photosynthetic purple bacterium *Rhodobacter sphaeroides* R-26.[63-66] Here, the principal components of the nqc tensors of the hydrogen-bonded deuterons and their principal directions with respect to the molecular axes of the quinone (defined by the two carbonyl groups) were obtained by spectral simulations of ENDOR spectra from frozen solutions of deuterium-exchanged samples recorded at different magnetic fields. From the comparison of these values with empirical linear relationships proposed in the literature,[67] the precise hydrogen bond lengths could be obtained. Another more recent example for an assignment of the length of a hydrogen bond via the nqc is the H-bond to the menasemiquinone radical in *Escherichia coli* nitrate reductase A.[68]

In the present case, nqcs of covalent C–^{2}H bonds in the flavin radical have been investigated. The values of 100 kHz and –20 kHz for ^{2}H(6) and ^{2}H(9) (Table 2), respectively, compare reasonably well with data reported for a deuterated organic model compound (~95 kHz),[69] however, the question arises why there is such a large difference between the two nuclei. In

principle, only contributions from electrons at the central atom exhibiting a nuclear quadrupolar moment have to be taken into account. For the ^{2}H atom, however, there is only a one-directional field gradient as the ^{2}H atom has only the 1s-orbital populated, which is transformed to a distorted directional sp^2 hybrid orbital in a C–^{2}H bond. Hence, to describe the nqc observed in the FMN radical, the nuclei and charge density elsewhere in the isoalloxazine moiety must be considered. The major contribution to the quadrupole tensor is supposed to be from the respective bonding partners, C(6) and C(9), because of the $1/r^3$ dependence of the quadrupolar tensor elements.[70] Therefore, the differences of the nqc of ^{2}H(6) and ^{2}H(9) can directly be correlated to their local spin density and thus, to their A_iso values (Table 1).

Temperature dependence of the 7α methyl group rotation

W-band Mims-ENDOR of the [7α,9-^{2}H$_4$]LOV* sample, recorded at 120 K and 20 K, afforded tensors of remarkably different shapes (see Figures 4 and 5). We assume a comparable behavior of the protons (deuterons) attached to C(8α) and C(7α) if samples are cooled down from 120 K to 20 K. In our model, the deuterated methyl group attached to C(7) does not rotate at 20 K within the time scale of the Mims-ENDOR experiment, which is reflected by three individual hf tensors of rhombic symmetry. On the other hand, methyl group rotation is fast at 120 K, and consequently, the three deuterons become magnetically equivalent and merge to one single hf tensor of axial symmetry.

In general, the temperature behavior of LOV* is highly unusual as most of the flavoprotein radicals investigated up to date show no restriction in methyl-group rotation at around 80 K.[5] Two different effects could be responsible for the pronounced temperature behavior of each of the two methyl groups in LOV*: either close-by amino acids interact with the methyl groups, or

the methyl groups influence each other. In case the first effect is dominant, differences in the temperature behavior of the two methyl groups are expected as their direct surroundings differ significantly: Three amino acids, namely L496 and in particular N425 and F509, are close to the 8α methyl group and are known to influence its rotation significantly.[33] On the other hand, a number of amino acids (T418, L496, F509, I510 and G511) are within a 4-Å distance to the 7α-methyl group and form a hydrophobic cavity;[71-72] however, no obvious protein cofactor interactions can be detected based on crystallographic data.[73] Nonetheless, W-band Mims-ENDOR data demonstrated a comparable temperature behavior of both methyl groups, although it has to be mentioned in this context that X-band Davies ENDOR and W-band Mims ENDOR data cannot be compared quantitatively as the extent of orientation selection and sensitivity towards motional dynamics is different in both methods.

Quantum-chemical calculations at the DFT level demonstrate a robust dependence of the rotational energies of the two methyl groups: Calculations of isoalloxazine radicals with both methyl groups present resulted in a rotational barrier of ~570–750 K (see Supporting Information and also Ref. [34]). If either of the two methyl groups is removed, the barrier is decreased drastically to ~20 K (see SI for details), thus indicating that the direct interaction of the two methyl groups is the dominant interaction (Figure S7). This finding is further corroborated by experimental data comparing the proton ranges of the X-band Davies-ENDOR spectra of unlabeled LOV* and [7α,9-^{2}H$_4$]LOV* samples (Figure 6). Since the protein environment is identical in both samples, the only difference is the proton-to-deuteron exchange at positions 7α and 9. Isotope labeling is not expected to redistribute the electron spin density of the isoalloxazine moiety, and therefore, the 8α proton hfcs remain unchanged upon deuteration of the protons at C(7α) and C(9). Consequently, the observed small differences in the ENDOR

signal patterns confirm that the temperature dependence of the two methyl groups are correlated, and more importantly, can be modulated by H/D exchange. In detail, shifts of the two 8α proton hfcs at 150 K can be explained by a slightly altered 8α methyl group rotation frequency. Two explanations can account for this finding: (i), a reduced interaction of the two methyl groups due to the ~2% shortened length of a C–D bond as compared to a C–H bond,[74] and (ii), a slower rotation frequency of the 7α CD$_3$ group as compared to a 7α CH$_3$ group arising from its enhanced moment of inertia. To receive further information on the interaction between the two methyl groups, DFT calculations with slight variations of (i), the C–H bond length (Figure S5), (ii), the rotational barrier of the 8α methyl group with respect to the dihedral angle (C(8)–C(7)–C(7α)–H(7α), Figure S6), and (iii), the rotational barrier of the 8α methyl group with respect to the bond angle (C(8)–C(7)–C(7α), Figure S7), were calculated. It turned out that reduction of the C–H bond length by 2% leads to a decrease of the rotational barrier by 10 K (Figure S5). More importantly, if the bond angle (C(8)–C(7)–C(7α) is changed only by 4°, an even more drastic alteration of the barrier height (about ± ~ 200 K) is achieved (Figures S7).

At 50 K, on the other hand, multiple shifts of H(8α) hfcs (lower panel of Figure 6) can without any doubt be assigned to changes of the angles of the arrested C(8α)–H bonds with respect to the isoalloxazine's ring plane. These angles have already been determined using DFT calculations;[33] unfortunately, the changes are small (around a few degrees) and thus, are below the uncertainties of our DFT calculations, which precludes a more quantitative analysis. In general, it should be noted that the differences between deuterated and unlabelled samples are close to threshold of detection, and therefore, only qualitative results can be discussed.

In sum, this ENDOR experiment remarkably demonstrates that the energy landscape of the two methyl groups is coupled and can be modulated by very small changes. Moreover, it confirms that only the protons attached to C(8α) are directly influenced by their surrounding amino acids, mostly by N425 and F509, and, on the other hand, the protons at C(7α) do not show any discernible protein-cofactor interactions. As the direct interaction between the two methyl groups is expected to be similar in all flavoproteins, the unusual temperature behavior in *A. sativa* LOV2 domains can be assigned to strong protein-cofactor interactions of the 8α protons, which apparently reduce the distance between the two methyl groups and, consequently, increase the rotational barrier. It will be interesting to see, whether the observed effect can also be found in other flavoproteins, or is unique for the flavin cofactor in *A. sativa* LOV2 domains.

Moreover, the question remains if this unusually strong interaction is required for LOV photoreceptor functioning/tuning. First hints that this interaction might indeed be relevant for its photochemistry has been given by a recent study showing that if the 8α methyl group is exchanged to an 8-bromo group, the stability of the photoadduct is drastically reduced.[75]

Conclusions

In this contribution, we describe how high-field ENDOR spectroscopy in combination with selective deuterium labeling leads to a more detailed picture of the electronic structure of flavin radicals. Supported by spectral simulations, all small deuteron hyperfine and quadrupole couplings could be ascertained with high precision; the in parts unexpected values are discussed in detail. Moreover, the temperature behavior of the 7α methyl group rotation was analyzed in greater detail, and a pronounced interplay between both methyl groups was detected. With the

help of selective deuterium editing, minute changes of the interaction between the two methyl groups could be probed by ENDOR spectroscopy, and a general picture of the methyl-group interactions could be drawn. Overall, the presented ENDOR data demonstrate that small changes in the local environment can be probed by measuring hfcs and that ENDOR spectroscopy is a suitable and sensitive method to probe tiny changes around a radical.
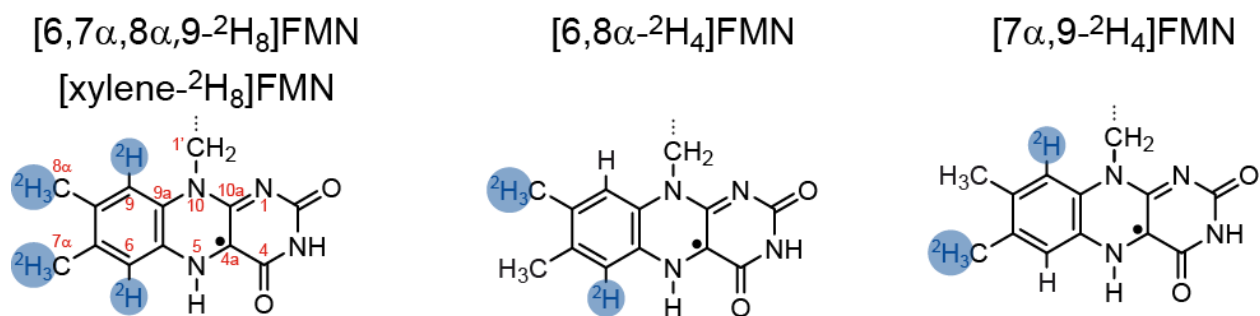
Scheme 1. Structure and IUPAC numbering of a neutral FMN radical. The labeling positions of the three used deuterium isotopologs are highlighted in blue.
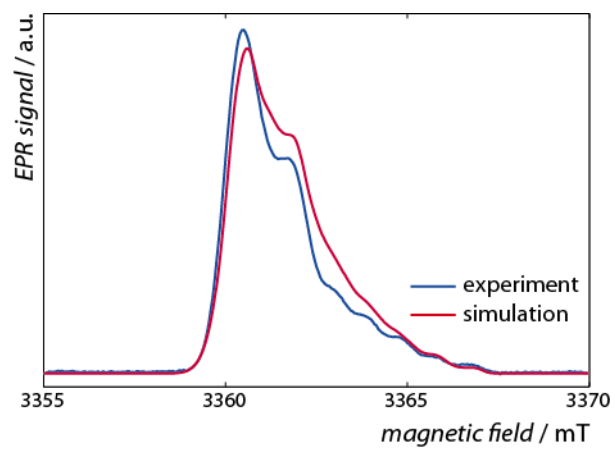
Figure 1. Pulsed W-band EPR spectrum of [xylene-^{2}H$_8$]LOV* (blue line) recorded at 80 K and its spectral simulation (red line).
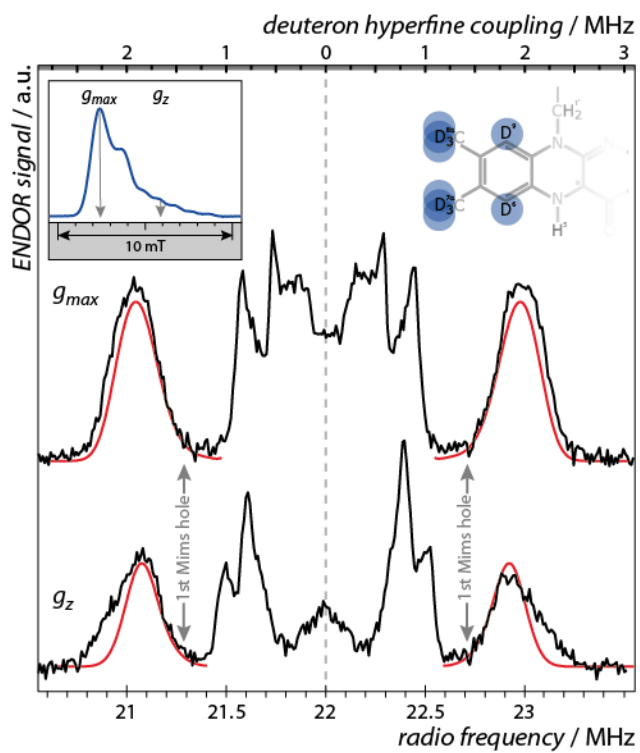
Figure 2. Pulsed W-band Mims-ENDOR spectra of [xylene-^{2}H$_8$]LOV* recorded at 20 K and magnetic-field positions corresponding to g_{max} (upper panel) and g_z (lower panel). The respective spectral simulations of two deuterons attached to C(8α) are depicted in red. Mims holes corresponding to a τ value of 700 ns are marked.
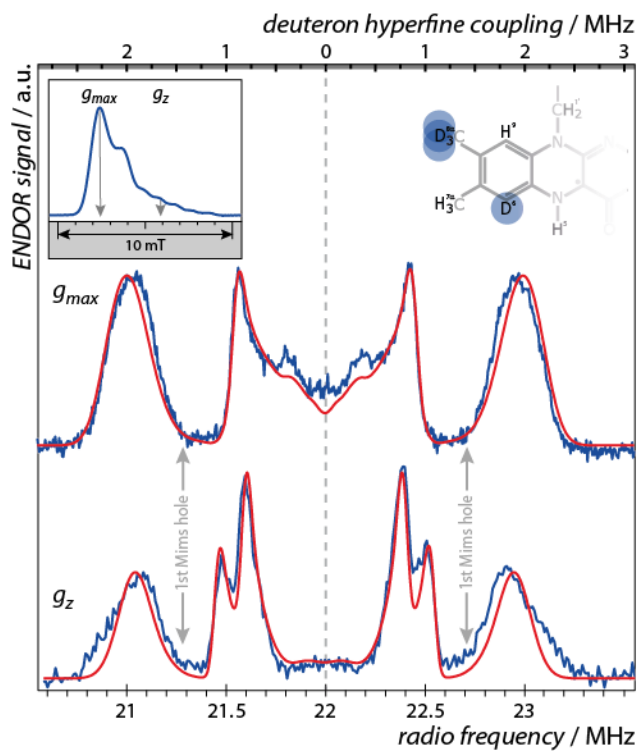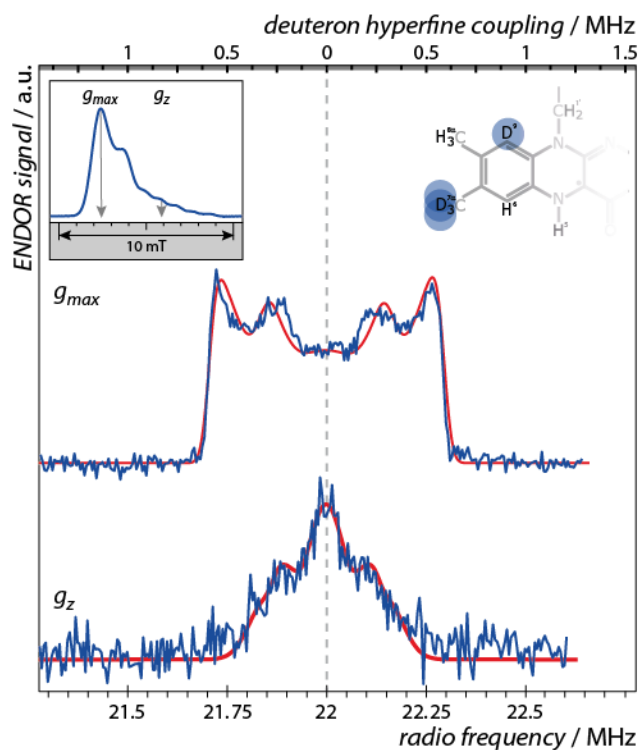
Figure 3. Pulsed W-band Mims-ENDOR spectra of [6,8α-^{2}H$_4$]LOV* recorded at 20 K and magnetic-field positions corresponding to g_{max} (upper panel) and g_z (lower panel). The respective spectral simulations of ^{2}H(6) and ^{2}H(8α) are depicted in red. Mims holes corresponding to a τ value of 700 ns are marked with an arrow.

Figure 4. Pulsed W-band Mims-ENDOR spectrum of [7α,9-^{2}H$_4$]LOV* recorded at 20 K and magnetic-field positions corresponding to g_{max} (upper panel) and g_z (lower panel), respectively. Spectral simulations of ^{2}H(7α) and ^{2}H(9) are depicted in red.
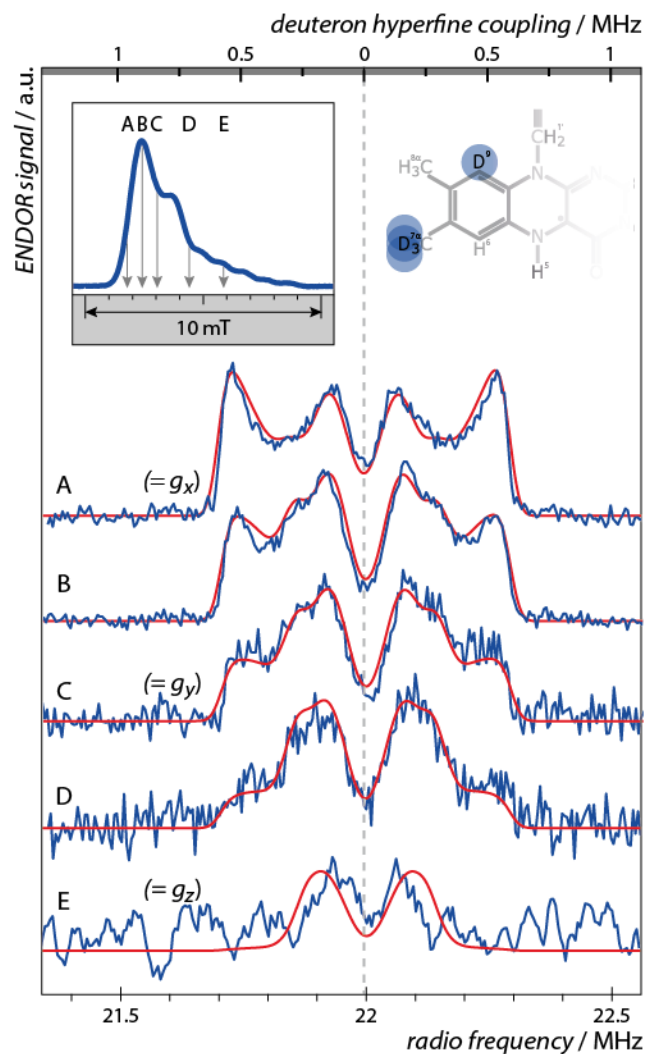
Figure 5: Pulsed W-band Mims-ENDOR spectrum of [7α,9-^{2}H$_4$]LOV* recorded at 120 K and magnetic-field positions corresponding to those indicated in the inset (spectra A–E). Spectral simulations are shown in red.
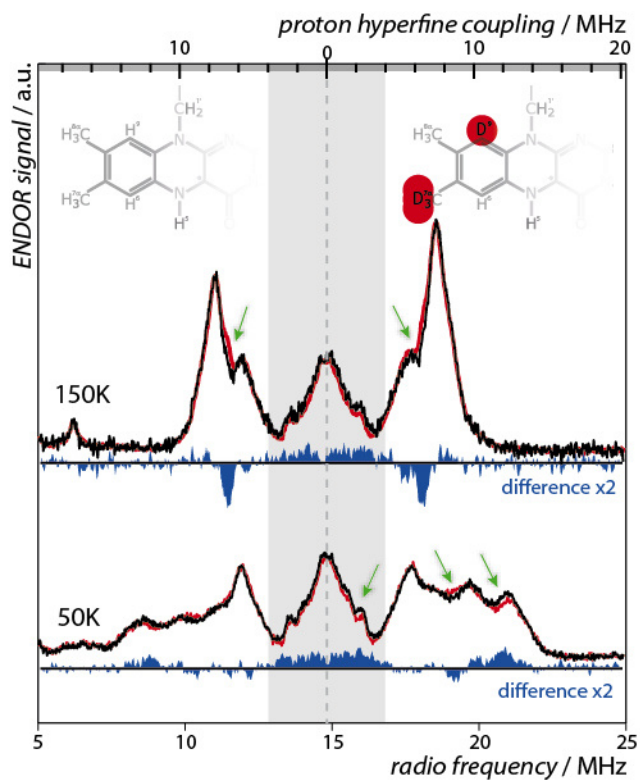
Figure 6: Scaled pulsed X-band Davies-ENDOR spectra of unlabeled LOV* (black) and [7α,9-²H₄]LOV* (red) recorded at 150 K and 50 K. Differences between the spectra are shown in blue, the matrix region is shown in gray. Differences between spectra obtained from an unlabeled and a deuterated FMN are highlighted by green arrows. For further details, see text.

Table 1. Deuteron hfcs of the FMNH$^\bullet$ cofactor obtained from simulations of pulsed Mims-ENDOR spectra of selectively cofactor labeled mutant *As*LOV2 domains measured at 20 or 120 K. All values in MHz; signs of hfcs have not been determined experimentally, but were taken from theoretical calculations.[39] Error bars were determined manually and individually based on the quality of the spectral simulation.

Hyperfine couplings /MHz						
Deuteron	A_{iso} (20 K)	A_{iso} (120 K) (scaled from proton hfcs)		A_x	A_y	A_z
^{2}H(6)	−0.51 ± 0.03	---		−0.90 ± 0.02	0.30 ± 0.03	−0.94 ± 0.02
^{2}H(7α)$_1$	0.26 ± 0.03	0.14 ± 0.05	−0.09 ± 0.05	0.18± 0.02	0.30 ± 0.03	0.31 ± 0.02
^{2}H(7α)$_2$	0.06 ± 0.04		0.03 ± 0.05	0.06± 0.02	0.08 ± 0.04	0.04 ± 0.02
^{2}H(7α)$_3$	0.06 ± 0.04		0.21 ± 0.05	0.06 ± 0.02	0.08 ± 0.04	0.04 ± 0.02
^{2}H(8α)$_1$	1.97 ± 0.02			1.77± 0.02	1.90 ± 0.02	2.21 ± 0.01
^{2}H(8α)$_2$	1.57 ± 0.02			1.26± 0.02	1.55 ± 0.02	1.77 ± 0.02
^{2}H(8α)$_3$	0.08 ± 0.3			−0.32± 0.3	+0.25± 0.3	+0.18± 0.3
^{2}H(9)	−0.01 ± 0.03	---		−0.59± 0.02	0.33± 0.03	0.21± 0.02

Scaled to proton hfcs (multiplied by 6.511)						
"Proton"	A_{iso} (20K)	A_{iso} (120K)		A_x	A_y	A_z
^{1}H(6)	−3.34± 0.15	---		−5.85	1.7	−6.15
^{1}H(7α)$_1$	1.71± 0.15	0.91	−0.59	1.17	1.95	2.01
^{1}H(7α)$_2$	0.39± 0.20		0,20	0.39	0.52	0.26
^{1}H(7α)$_3$	0.39± 0.20		1,37	0.39	0.52	0.26
^{1}H(8α)$_1$	12.8± 0.07*	7.90± 0.10*	7.0*	11.5	12.4	14.4
^{1}H(8α)$_2$	10.2± 0.07*		7.0*	8.2	10.1	11.5
^{1}H(8α)$_3$	0.5± 0.65*		9.3*	−2.1	1.6	1.2
^{1}H(9)	−0.11± 0.15	---		−3.84	2.15	1.37

*taken from [33]

Table 2. Nuclear quadrupole couplings of the deuterons ^{2}H(6) and ^{2}H(9) obtained from simulations of pulsed Mims-ENDOR spectra of selective FMN-labeled mutant *As*LOV2 domains measured at 20 K. All values in MHz; signs of hfcs have not been determined experimentally, but were taken from spectral simulations. Error bars were determined manually and individually based on the quality of the spectral simulation.

Quadruple couplings					
Deuteron	Q /MHz	η	P_x /MHz	P_y /MHz	P_z /MHz
^{2}H(6)	0.10 ± 0.01	0.8 ± 0.1	< 0.04± 0.01	0.120± 0.04	0.120± 0.01
^{2}H(9)	−0.02 ± 0.01	−0.8 ± 0.1	< 0.04± 0.01	< 0.04± 0.01	< 0.04± 0.01

AUTHOR INFORMATION

Corresponding Author

* *E-mail:* erik.schleicher@physchem.uni-freiburg.de. *Phone: +49 (0)761 203 6204;*

Fax: +49 (0)761 203 6222.

Author Contributions

R.Br., M.F., S.W., A.B., R.Bi. and E.S. designed the research and planned the experiments. B.I. produced and purified the protein samples. R.-R.K. synthesized the flavin isotopoloques. L.H. performed the DFT calculations. R.Br. performed the EPR/ENDOR experiments. R.Br. and E.S. analyzed the data and performed the spectral simulations. R.B. and E.S. wrote the paper with input from all other authors.

Notes

The authors declare no competing financial interest.

ASSOCIATED CONTENT

Supporting Information. The following files are available.

A) Supporting Information for ENDOR spectroscopy (Figures S1–S3)

B) Supporting Information for DFT calculations (Tables S1–S4 and Figures S4–S7)

C) Supporting information of the synthesis of deuterated riboflavins (Tables S5–S6 and Figures S8–S10)

This information is available free of charge via the Internet at http://pubs.acs.org

REFERENCES

1.   Massey, V., The chemical and biological versatility of riboflavin. *Biochemical Society Transactions* **2000,** *28*, 283-296.
2.   Joosten, V.; van Berkel, W. J. H., Flavoenzymes. *Current Opinion in Chemical Biology* **2007,** *11*, 195-202.
3.   Fraaije, M. W.; Mattevi, A., Flavoenzymes: diverse catalysts with recurrent features. *Trends in Biochemical Sciences* **2000,** *25*, 126-132.
4.   Rostas, A.; Einholz, C.; Illarionov, B.; Heidinger, L.; Al Said, T.; Bauss, A.; Fischer, M.; Bacher, A.; Weber, S.; Schleicher, E., Long-lived hydrated FMN radicals: EPR characterization and implications for catalytic variability in flavoproteins. *Journal of the American Chemical Society* **2018,** *140*, 16521-16527.
5.   Schleicher, E.; Wenzel, R.; Ahmad, M.; Batschauer, A.; Essen, L.-O.; Hitomi, K.; Getzoff, E. D.; Bittl, R.; Weber, S.; Okafuji, A., The electronic state of flavoproteins: investigations with proton electron–nuclear double resonance. *Applied Magnetic Resonance* **2010,** *37*, 339-352.
6.   Schleicher, E.; Weber, S., Radicals in flavoproteins. *Topics in Current Chemistry* **2012,** *321*, 41-66.
7.   Nohr, D.; Weber, S.; Schleicher, E., EPR spectroscopy on flavin radicals in flavoproteins. In *New Approaches for Flavin Catalysis*, Palfey, B. A., Ed. Elsevier: 2019; Vol. 620, pp 251 - 275.
8.   Martínez, J. I.; Alonso, P. J.; Medina, M., The electronic structure of the neutral isoalloxazine semiquinone within *Anabaena* flavodoxin: new insights from HYSCORE experiments. *Journal of Magnetic Resonance* **2012,** *218*, 153-162.
9.   Harmer, J. R., Hyperfine spectroscopy – ENDOR. *eMagRes* **2016,** *5*, 1493-1514.
10.   Murphy, D. M.; Farley, R. D., Principles and applications of ENDOR spectroscopy for structure determination in solution and disordered matrices. *Chemical Society Reviews* **2006,** *35*, 249-268.
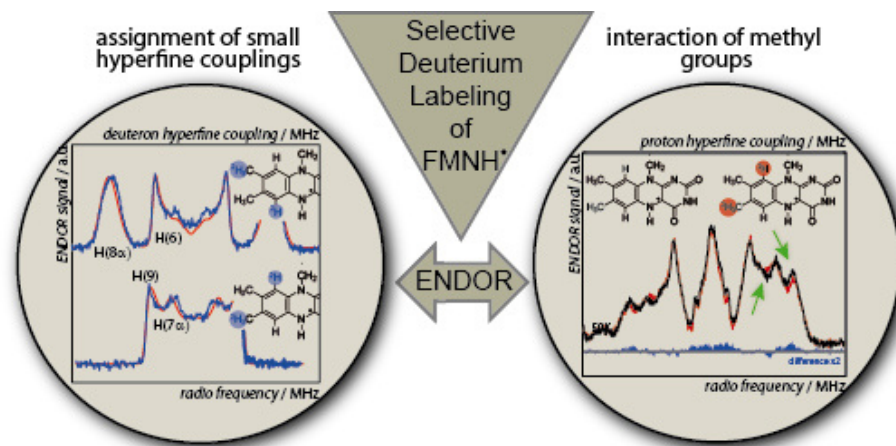
11. Medina, M.; Lostao, A.; Sancho, J.; Gómez-Moreno, C.; Cammack, R.; Alonso, P. J.; Martínez, J. I., Electron-nuclear double resonance and hyperfine sublevel correlation spectroscopic studies of flavodoxin mutants from *Anabaena* sp. PCC 7119. *Biophysical Journal* **1999,** *77*, 1712-1720.

12. Medina, M.; Vrielink, A.; Cammack, R., Electron spin echo envelope modulation studies of the semiquinone anion radical of cholesterol oxidase from *Brevibacterium sterolicum*. *FEBS Letters* **1997,** *400*, 247-251.

13. Barquera, B.; Ramirez-Silva, L.; Morgan, J. E.; Nilges, M. J., A new flavin radical signal in the Na^+-pumping NADH:quinone oxidoreductase from *Vibrio cholerae*. An EPR/electron nuclear double resonance investigation of the role of the covalently bound flavins in subunits B and C. *Journal of Biological Chemistry* **2006,** *281*, 36482-36491.

14. Weber, S.; Kay, C. W. M.; Bacher, A.; Richter, G.; Bittl, R., Probing the N(5)–H bond of the isoalloxazine moiety of flavin radicals by X- and W-band pulsed electron–nuclear double resonance. *ChemPhysChem* **2005,** *6*, 292-299.

15. Kulik, L. V.; Pivtsov, A. V.; Bogachev, A. V., Pulse EPR, ENDOR, and ELDOR study of anionic flavin radicals in Na^+-translocating NADH:quinone oxidoreductase. *Applied Magnetic Resonance* **2010,** *37*, 353-361.

16. Kay, C. W. M.; Grishin, Y. A.; Weber, S.; Möbius, K., An improved TM_{110} resonator for continuous-wave ENDOR studies at X-band. *Applied Magnetic Resonance* **2007,** *31*, 599-609.

17. Schnegg, A.; Okafuji, A.; Bacher, A.; Bittl, R.; Fischer, M.; Fuchs, M. R.; Hegemann, P.; Joshi, M.; Kay, C. W. M.; Richter, G.; Schleicher, E.; Weber, S., Towards an identification of chemically different flavin radicals by means of their *g*-tensor. *Applied Magnetic Resonance* **2006,** *30*, 345-358.

18. Zoltowski, B. D.; Gardner, K. H., Tripping the light fantastic: blue-light photoreceptors as examples of environmentally modulated protein–protein interactions. *Biochemistry* **2011,** *50*, 4-16.

19. Losi, A.; Gärtner, W., The evolution of flavin-binding photoreceptors: an ancient chromophore serving trendy blue-light sensors. *Annual Review of Plant Biology* **2012,** *63*, 49-72.

20. Briggs, W. R., The LOV domain: a chromophore module servicing multiple photoreceptors. *Journal of Biomedical Science* **2007,** *14*, 499-504.

21. Christie, J. M., Phototropin blue-light receptors. *Annual Review of Plant Biology* **2007,** *58*, 21-45.

22. Mi, Q.; Ratner, M. A.; Wasielewski, M. R., Time-resolved EPR spectra of spin-correlated radical pairs: spectral and kinetic modulation resulting from electron–nuclear hyperfine interactions. *Journal of Physical Chemistry A* **2010,** *114*, 162-171.

23. Briggs, W. R.; Christie, J. M., Phototropins 1 and 2: versatile plant blue-light receptors. *Trends in Plant Science* **2002,** *7*, 204-210.

24. Swartz, T. E.; Tseng, T.-S.; Frederickson, M. A.; Paris, G.; Comerci, D. J.; Rajashekara, G.; Kim, J.-G.; Mudgett, M. B.; Splitter, G. A.; Ugalde, R. A.; Goldbaum, F. A.; Briggs, W. R.; Bogomolni, R. A., Blue-light–activated histidine kinases: two-component sensors in bacteria. *Science* **2007,** *317*, 1090-1093.

25. Suzuki, N.; Takaya, N.; Hoshino, T.; Nakamura, A., Enhancement of a σ^B-dependent stress response in *Bacillus subtilis* by light via YtvA photoreceptor. *Journal of General and Applied Microbiology* **2007,** *53*, 81-88.

26. Salomon, M.; Christie, J. M.; Knieb, E.; Lempert, U.; Briggs, W. R., Photochemical and mutational analysis of the FMN-binding domain of the plant blue light receptor, phototropin. *Biochemistry* **2000,** *39*, 9401-9410.

27. Crosson, S.; Moffat, K., Photoexcited structure of a plant photoreceptor domain reveals a light-driven molecular switch. *Plant Cell* **2002,** *14*, 1067-1075.

28. Schleicher, E.; Kowalczyk, R. M.; Kay, C. W. M.; Hegemann, P.; Bacher, A.; Fischer, M.; Bittl, R.; Richter, G.; Weber, S., On the reaction mechanism of adduct formation in LOV domains of the plant blue-light receptor phototropin. *Journal of the American Chemical Society* **2004,** *126*, 11067-11076.

29. Kay, C. W. M.; Schleicher, E.; Kuppig, A.; Hofner, H.; Rüdiger, W.; Schleicher, M.; Fischer, M.; Bacher, A.; Weber, S.; Richter, G., Blue light perception in plants. Detection and characterization of a light-induced neutral flavin radical in a C450A mutant of phototropin. *Journal of Biological Chemistry* **2003,** *278*, 10973-10982.

30. Lanzl, K.; von Sanden-Flohe, M.; Kutta, R.-J.; Dick, B., Photoreaction of mutated LOV photoreceptor domains from *Chlamydomonas reinhardtii* with aliphatic mercaptans: implications for the mechanism of wild type LOV. *Physical Chemistry Chemical Physics* **2010,** *12*, 6594-6604.

31. Kottke, T.; Heberle, J.; Hehn, D.; Dick, B.; Hegemann, P., Phot-LOV1: photocycle of a blue-light receptor domain from the green alga *Chlamydomonas reinhardtii*. *Biophysical Journal* **2003,** *84*, 1192-1201.

32. Kopka, B.; Magerl, K.; Savitsky, A.; Davari, M. D.; Röllen, K.; Bocola, M.; Dick, B.; Schwaneberg, U.; Jaeger, K.-E.; Krauss, U., Electron transfer pathways in a light, oxygen, voltage (LOV) protein devoid of the photoactive cysteine. *Scientific Reports* **2017,** *7*, Art.-No. 13346.

33. Brosi, R.; Illarionov, B.; Mathes, T.; Fischer, M.; Joshi, M.; Bacher, A.; Hegemann, P.; Bittl, R.; Weber, S.; Schleicher, E., Hindered rotation of a cofactor methyl group as a probe for protein–cofactor interaction. *Journal of the American Chemical Society* **2010,** *132*, 8935-8944.

34. Martínez, J. I.; Alonso, P. J.; García-Rubio, I.; Medina, M., Methyl rotors in flavoproteins. *Physical Chemistry Chemical Physics* **2014,** *16*, 26203-26212.

35. Diensthuber, R. P.; Engelhard, C.; Lemke, N.; Gleichmann, T.; Ohlendorf, R.; Bittl, R.; Möglich, A., Biophysical, mutational, and functional investigation of the chromophore-binding pocket of light-oxygen-voltage photoreceptors. *ACS Synthetic Biology* **2014,** *3*, 811-819.

36. Pompe, N.; Chen, J.; Illarionov, B.; Panter, S.; Fischer, M.; Bacher, A.; Weber, S., Methyl groups matter: photo-CIDNP characterizations of the semiquinone radicals of FMN and demethylated FMN analogs. *J. Chem. Phys.* **2019,** *151*, Art.No. 235103.

37. Beach, R. L.; Plaut, G. W. E., Investigations of structures of substituted lumazines by deuterium exchange and nuclear magnetic resonance spectroscopy. *Biochemistry* **1970,** *9*, 760-770.

38. Stoll, S.; Schweiger, A., EasySpin, a comprehensive software package for spectral simulation and analysis in EPR. *Journal of Magnetic Resonance* **2006,** *178*, 42-55.

39. Weber, S.; Möbius, K.; Richter, G.; Kay, C. W. M., The electronic structure of the flavin cofactor in DNA photolyase. *Journal of the American Chemical Society* **2001,** *123*, 3790-3798.

40. Neese, F. *ORCA. An ab initio, DFT and semiempirical electronic structure package*, Version 2.9; Max-Planck-Institut für Bioanorganische Chemie: Mülheim (Germany).

41.   Drennan, C. L.; Pattridge, K. A.; Weber, C. H.; Metzger, A. L.; Hoover, D. M.; Ludwig, M. L., Refined structures of oxidized flavodoxin from Anacystis nidulans. *Journal of Molecular Biology* **1999,** *294* (3), 711-724.

42.   Kay, C. W. M.; Schleicher, E.; Hitomi, K.; Todo, T.; Bittl, R.; Weber, S., Determination of the g-matrix orientation in flavin radicals by high-field/high-frequency electron-nuclear double resonance. *Magnetic Resonance in Chemistry* **2005,** *43*, S96-S102.

43.   Okafuji, A.; Schnegg, A.; Schleicher, E.; Möbius, K.; Weber, S., G-tensors of the flavin adenine dinucleotide radicals in glucose oxidase: a comparative multifrequency electron paramagnetic resonance and electron–nuclear double resonance study. *Journal of Physical Chemistry B* **2008,** *112*, 3568-3574.

44.   Barquera, B.; Morgan, J. E.; Lukoyanov, D.; Scholes, C. P.; Gennis, R. B.; Nilges, M. J., X- and W-band EPR and Q-band ENDOR studies of the flavin radical in the Na$^+$-translocating NADH:quinone oxidoreductase from *Vibrio cholerae*. *Journal of the American Chemical Society* **2003,** *125*, 265-275.

45.   Paulus, B.; Illarionov, B.; Nohr, D.; Roellinger, G.; Kacprzak, S.; Fischer, M.; Weber, S.; Bacher, A.; Schleicher, E., One protein, two chromophores: comparative spectroscopic characterization of 6,7-dimethyl-8-ribityllumazine and riboflavin bound to lumazine protein. *Journal of Physical Chemistry B* **2014,** *118*, 13092-13105.

46.   Fuchs, M.; Schleicher, E.; Schnegg, A.; Kay, C. W. M.; Törring, J. T.; Bittl, R.; Bacher, A.; Richter, G.; Möbius, K.; Weber, S., The g-tensor of the neutral flavin radical cofactor of DNA photolyase revealed by 360-GHz electron paramagnetic resonance spectroscopy. *Journal of Physical Chemistry B* **2002,** *106*, 8885-8890.

47.   García, J. I.; Medina, M.; Sancho, J.; Alonso, P. J.; Gómez-Moreno, C.; Mayoral, J. A.; Martínez, J. I., Theoretical analysis of the electron spin density distribution of the flavin semiquinone isoalloxazine ring within model protein environments. *Journal of Physical Chemistry A* **2002,** *106*, 4729-4735.

48.   Stoll, S.; Goldfarb, D., EPR Interactions – Nuclear Quadrupole Couplings. *eMagRes* **2017,** *6*, 495-510.

49.   Hunt, M. J.; Mackay, A. L., Deuterium and nitrogen pure quadrupole resonance in deuterated amino acids. *Journal of Magnetic Resonance* **1974,** *15*, 402-414.

50.   Doan, P. E.; Lees, N. S.; Shanmugam, M.; Hoffman, B. M., Simulating suppression effects in pulsed ENDOR, and the 'Hole in the Middle' of Mims and Davies ENDOR spectra. *Applied Magnetic Resonance* **2010,** *37*, 763-779.

51.   Harmer, J. R., Hyperfine Spectroscopy – ENDOR. *eMagRes* **2017,** *6*, 331-358.

52.   Kurreck, H.; Bretz, N. H.; Helle, N.; Henzel, N.; Weilbacher, E., ENDOR studies of flavins and flavoproteins. *Journal of the Chemical Society, Faraday Transactions 1* **1988,** *84*, 3293-3306.

53.   Kay, C. W. M.; El Mkami, H.; Molla, G.; Pollegioni, L.; Ramsay, R. R., Characterization of the covalently bound anionic flavin radical in monoamine oxidase A by electron paramagnetic resonance. *Journal of the American Chemical Society* **2007,** *129*, 16091-16097.

54.   Kay, C. W. M.; Feicht, R.; Schulz, K.; Sadewater, P.; Sancar, A.; Bacher, A.; Möbius, K.; Richter, G.; Weber, S., EPR, ENDOR and TRIPLE resonance spectroscopy on the neutral flavin radical in *Escherichia coli* DNA photolyase. *Biochemistry* **1999,** *38*, 16740-16748.

55.   Eriksson, L. E. G.; Ehrenberg, A., Electron spin resonance study on anionic flavin free radicals. *Acta Chemica Scandinavica* **1964,** *18*, 1437-1453.

56.   Eriksson, L. E. G.; Ehrenberg, A., On the powder ESR and ENDOR spectra of flavoprotein radicals. *Biochimica et Biophysica Acta* **1973,** *293*, 57-66.

57.   Pauwels, E.; Declerck, R.; Verstraelen, T.; De Sterck, B.; Kay, C. W. M.; Van Speybroeck, V.; Waroquier, M., Influence of protein environment on the electron paramagnetic resonance properties of flavoprotein radicals: a QM/MM study. *Journal of Physical Chemistry B* **2010,** *114*, 16655-16665.

58.   Butler, L. G.; Keiter, E. A., Interpretation of electric field gradients at deuterium as measured by solid-state NMR spectroscopy. *Journal of Coordination Chemistry* **1994,** *32*, 121-134.

59.   Huber, H., Deuterium quadrupole coupling constants. A theoretical investigation. *Journal of Chemical Physics* **1985,** *83*, 4591-4598.

60.   Ragle, J. L.; Mokarram, M.; Presz, D.; Minott, G., Quadrupole coupling of deuterium bonded to carbon. *Journal of Magnetic Resonance* **1975,** *20*, 195-213.

61.   Vold, R. L.; Hoatson, G. L.; Tse, T. Y., Effects of slow motion on deuteron relaxation time anisotropy. *Chemical Physics Letters* **1996,** *263*, 271-275.

62.   Parker Jr., W. O.; Hobley, J.; Malatesta, V., Quadrupole coupling parameters of olefinic deuterons: ^{2}H MAS NMR spectroscopy of photochromic spiropyran and merocyanines. *Journal of Physical Chemistry A* **2002,** *106*, 4028-4031.

63.   Flores, M.; Isaacson, R. A.; Calvo, R.; Feher, G.; Lubitz, W., Probing hydrogen bonding to quinone anion radicals by ^{1}H and ^{2}H ENDOR spectroscopy at 35 GHz. *Chemical Physics* **2003,** *294*, 401-413.

64.   Sinnecker, S.; Reijerse, E.; Neese, F.; Lubitz, W., Hydrogen bond geometries from electron paramagnetic resonance and electron–nuclear double resonance parameters: density functional study of quinone radical anion–solvent interactions. *Journal of the American Chemical Society* **2004,** *126*, 3280-3290.

65.   Sinnecker, S.; Flores, M.; Lubitz, W., Protein–cofactor interactions in bacterial reaction centers from *Rhodobacter sphaeroides* R-26: Effect of hydrogen bonding on the electronic and geometric structure of the primary quinone. A density functional theory study. *Physical Chemistry Chemical Physics* **2006,** *8*, 5659-5670.

66.   Flores, M.; Isaacson, R.; Abresh, E.; Calvo, R.; Lubitz, W.; Feher, G., Protein-cofactor interactions in bacterial reaction centers from *Rhodobacter sphaeroides* R-26: II. Geometry of the hydrogen bonds to the primary quinone $Q_A{}^{-}$ by ^{1}H and ^{2}H ENDOR spectroscopy. *Biophysical Journal* **2007,** *92*, 671-682.

67.   Soda, G.; Chiba, T., Deuteron magnetic resonance study of cupric sulfate pentahydrate. *Journal of Chemical Physics* **1969,** *50*, 439-455.

68.   Grimaldi, S.; Arias-Cartin, R.; Lanciano, P.; Lyubenova, S.; Szenes, R.; Endeward, B.; Prisner, T. F.; Guigliarelli, B.; Magalon, A., Determination of the proton environment of high stability Menasemiquinone intermediate in Escherichia coli nitrate reductase A by pulsed EPR. *J Biol Chem* **2012,** *287* (7), 4662-4670.

69.   Biehl, R.; Lubitz, W.; Möbius, K.; Plato, M., Observation of deuterium quadrupole splittings of aromatic free radicals in liquid crystals by ENDOR and TRIPLE resonance. *Journal of Chemical Physics* **1977,** *66*, 2074-2078.

70.   Sanderud, A.; Sagstuen, E.; Itagaki, Y.; Lund, A., EPR and ENDOR studies of deuteron hyperfine and quadrupole coupling in ·CD(COOD)$_2$: experimental and theoretical estimates of electric field gradients from an α-carbon. *Journal of Physical Chemistry A* **2000,** *104*, 6372-6379.

71.   Raffelberg, S.; Gutt, A.; Gärtner, W.; Mandalari, C.; Abbruzzetti, S.; Viappiani, C.; Losi, A., The amino acids surrounding the flavin 7a-methyl group determine the UVA spectral features of a LOV protein. *Biological Chemistry* **2013,** *394*, 1517-1528.

72.   Raffelberg, S.; Mansurova, M.; Gärtner, W.; Losi, A., Modulation of the photocycle of a LOV domain photoreceptor by the hydrogen-bonding network. *Journal of the American Chemical Society* **2011,** *133*, 5346-5356.

73.   Halavaty, A. S.; Moffat, K., N- and C-terminal flanking regions modulate light-induced signal transduction in the LOV2 domain of the blue light sensor phototropin 1 from *Avena sativa*. *Biochemistry* **2007,** *46*, 14001-14009.

74.   Ibberson, R. M.; Prager, M., The *ab initio* crystal structure determination of vapour-deposited methyl fluoride by high-resolution neutron powder diffraction. *Acta Crystallographica, Section B: Structural Science* **1996,** *B52*, 892-895.

75.   Mansurova, M.; Simon, J.; Salzmann, S.; Marian, C. M.; Gärtner, W., Spectroscopic and theoretical study on electronically modified chromophores in LOV domains: 8-bromo- and 8-trifluoromethyl-substituted flavins. *ChemBioChem* **2013,** *14*, 645-654.

TOC Figure